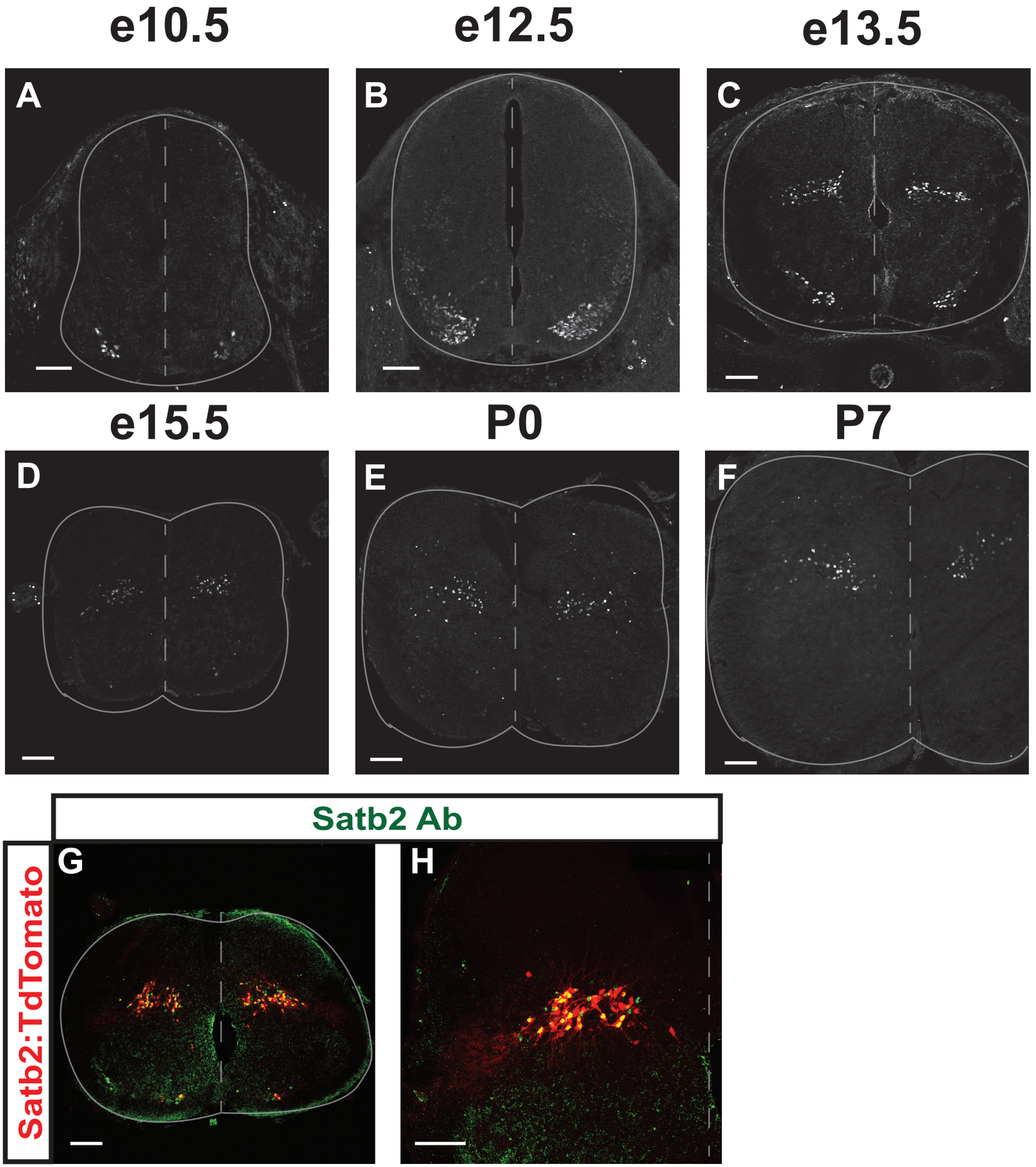
e10.5
e12.5
e13.5
A
B
C
e15.5
P0
P7
D
E
F
Satb2 Ab
Satb2:TdTomato
G
H

Lbx1
Lim1/2
Ptf1a-Cre
Pax2
Satb2
A
B
C
D
E
F
G
H
Bhlhb5
Isl1/2
Lmx1b-Cre
Brn3a
Satb2
I
J
K
L
M
N
O
P
GAD65
GAD67
vGlut2
Satb2
Q
R
S

Satb2:TdTomato PV vGlut1

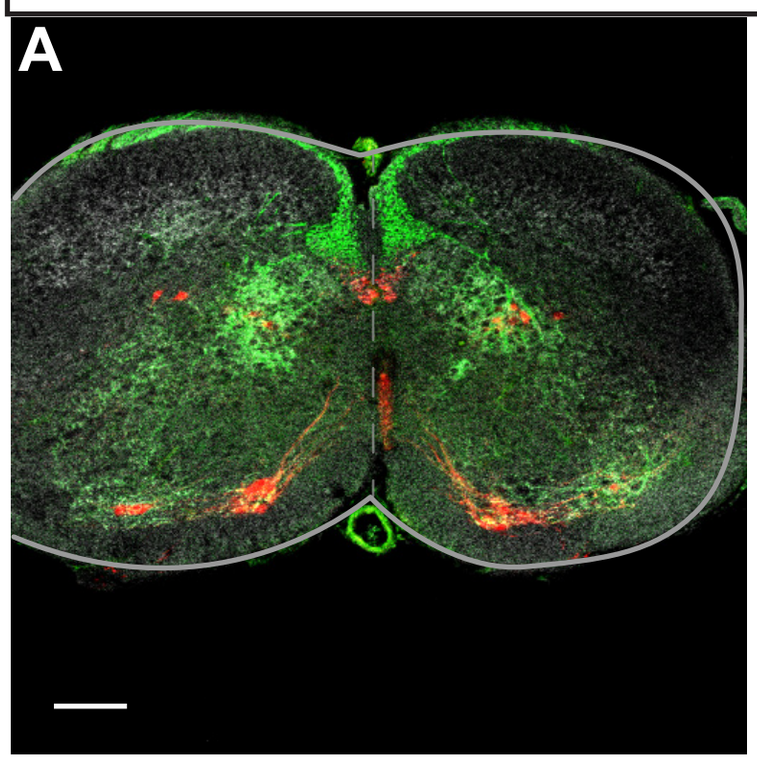

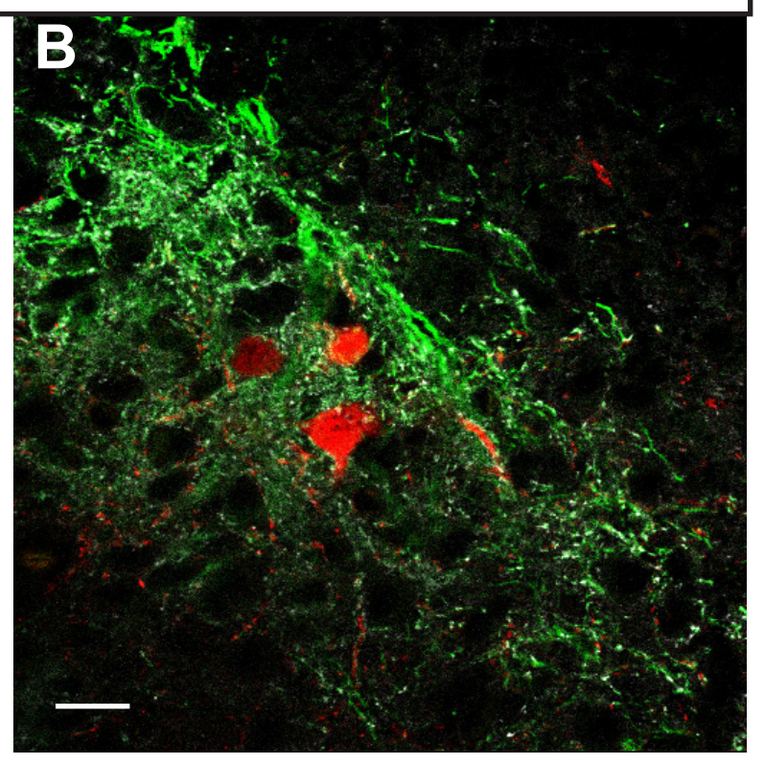

Lmx1b:Syn-Tom

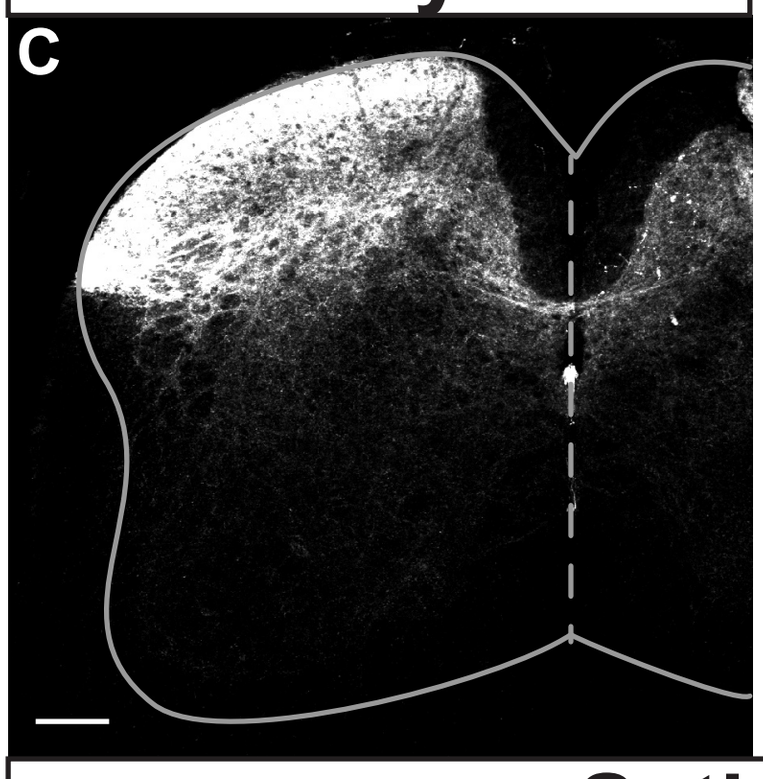

Ptf1a:Syn-Tom

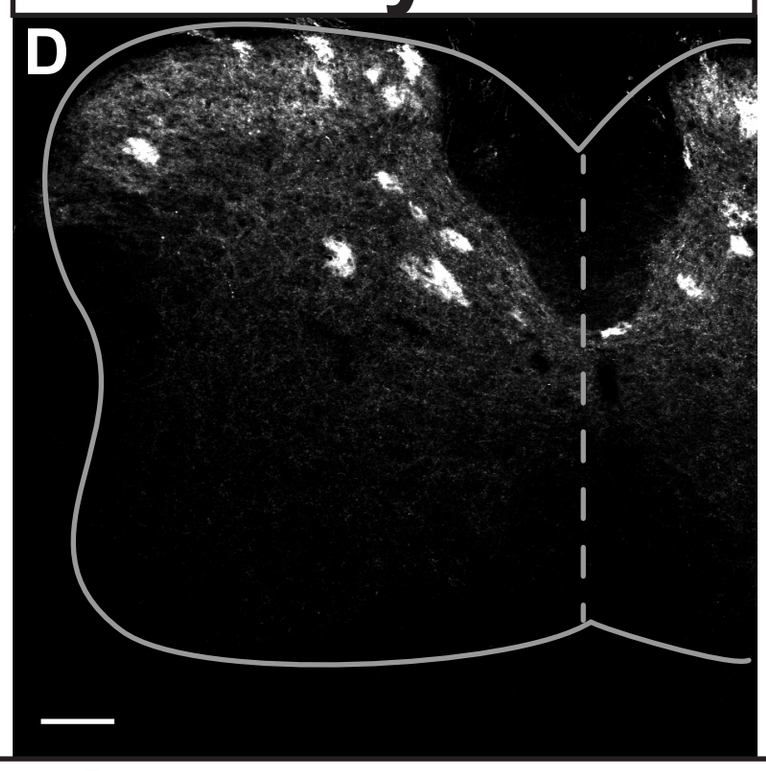

Satb2:Syn-Tom Neurotrace

Evx1 (V0c)

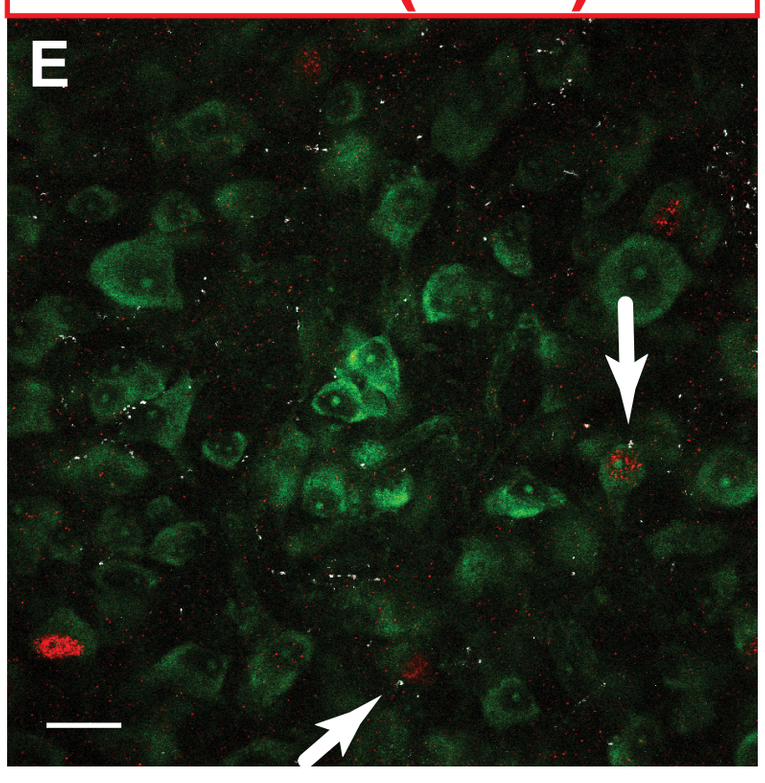

Calbindin (Mixed)

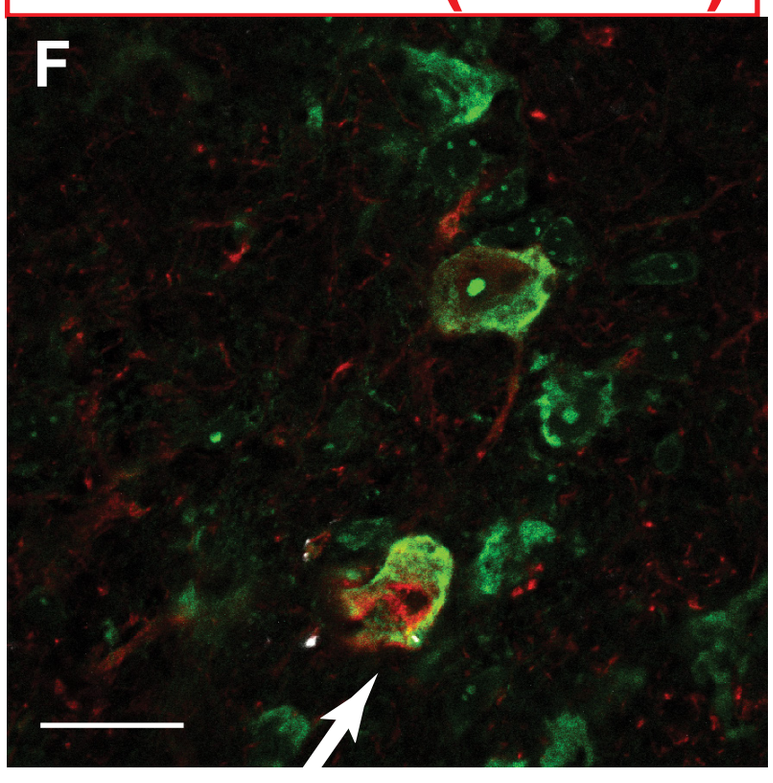

Bhlhb5 (Mixed)

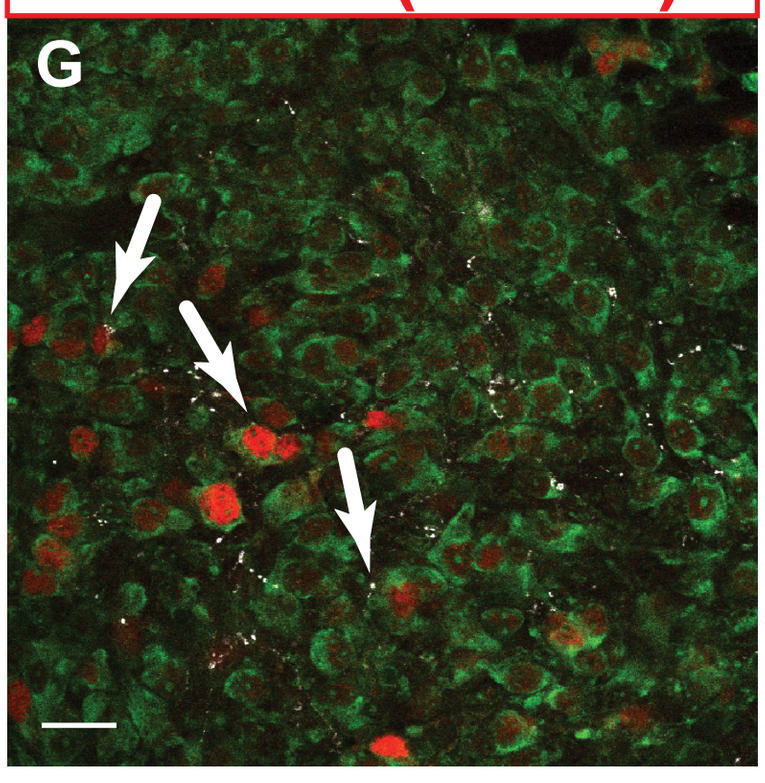

scAAV-Flex-GFP

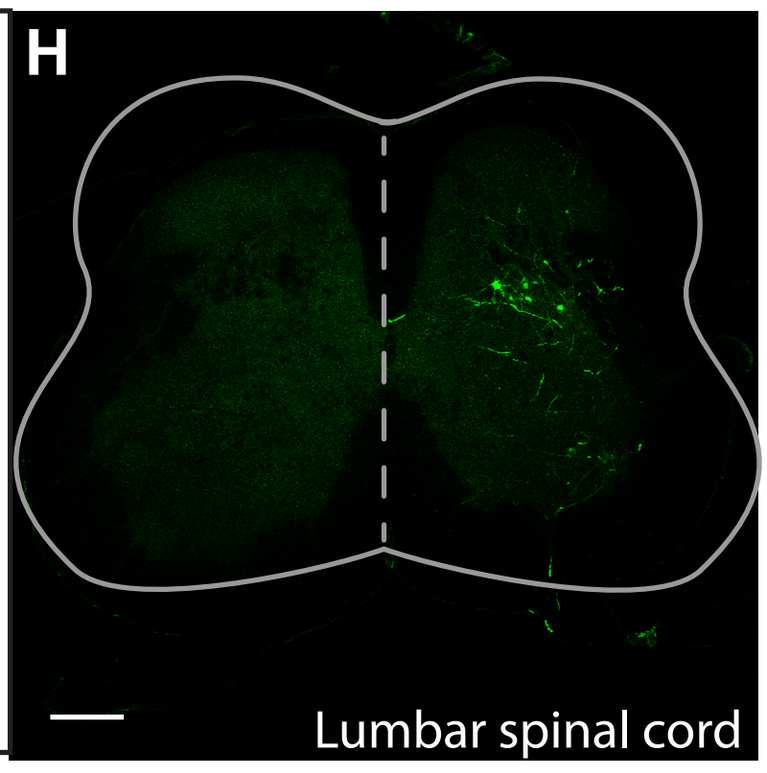

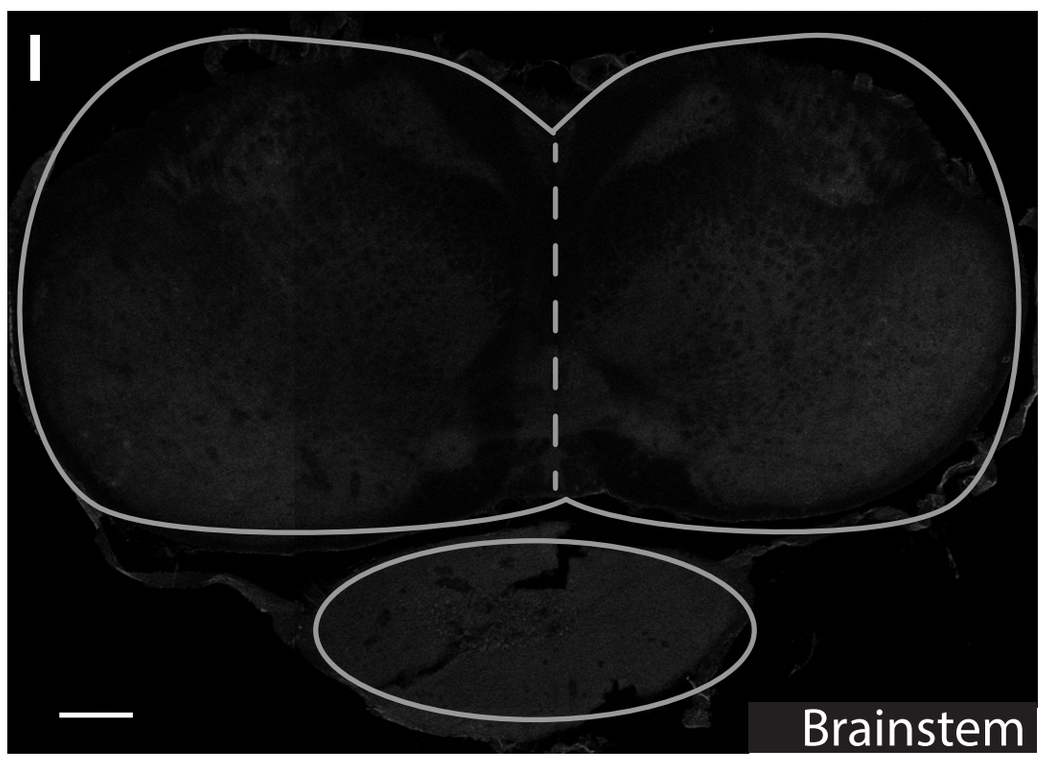

Control

ISR-*Satb2*^{KO}

Satb2^{KO}

Satb2 Ab

A

B

C

Satb2:TdTomato Lbx1 Hb9

Lbx1:TdTomato Hb9

Satb2^{KO}:TdTomato Hb9

D

E

F

A

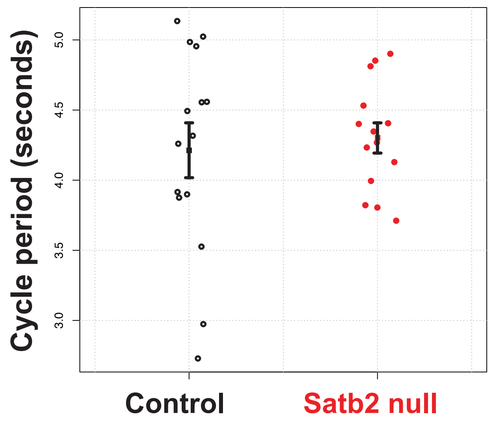

B

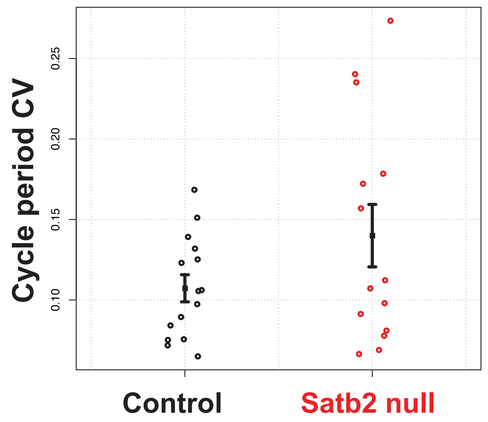

C

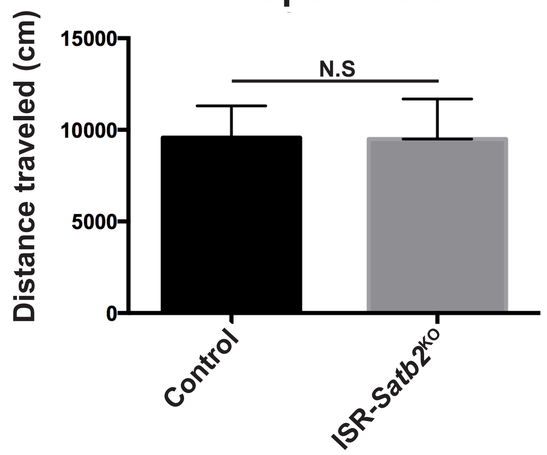

D

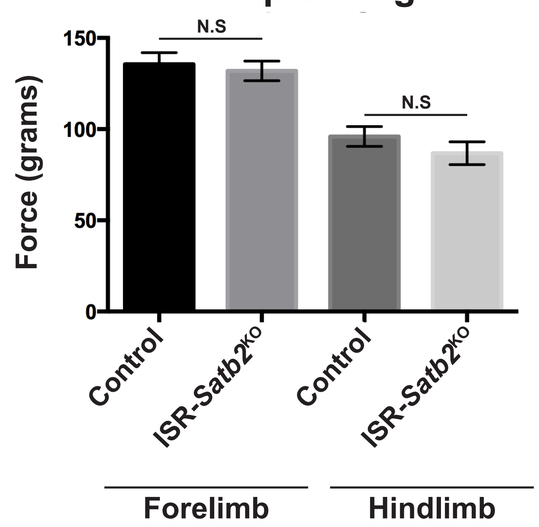

E

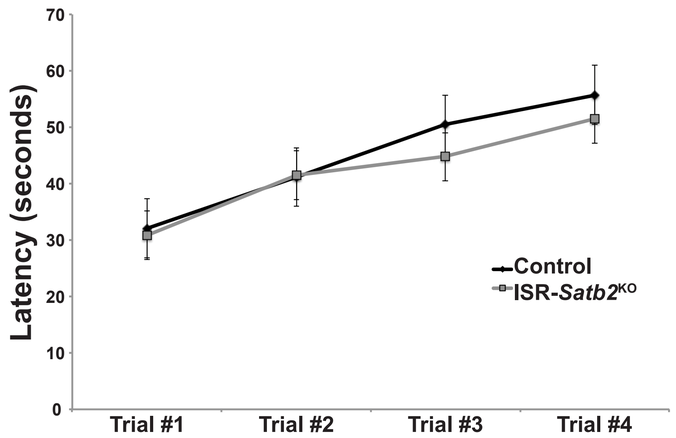

F

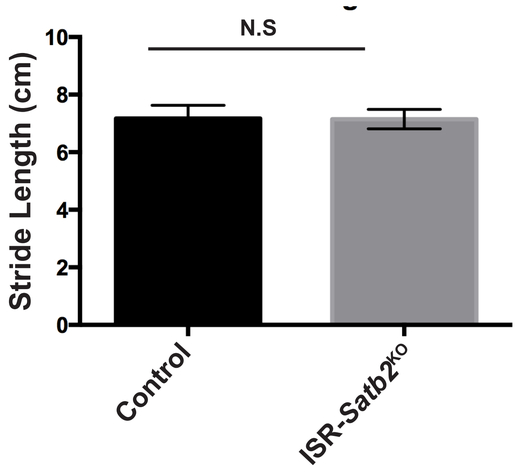

G

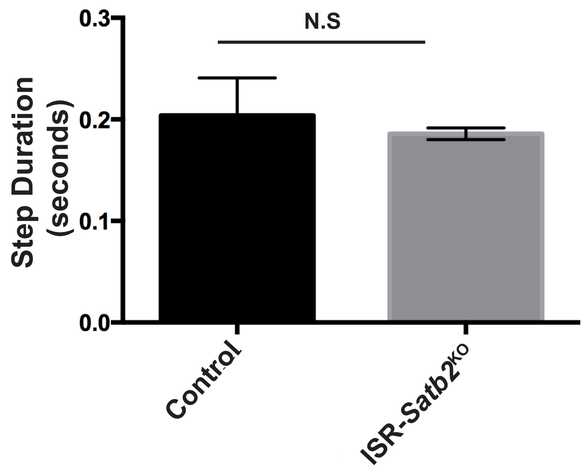

H

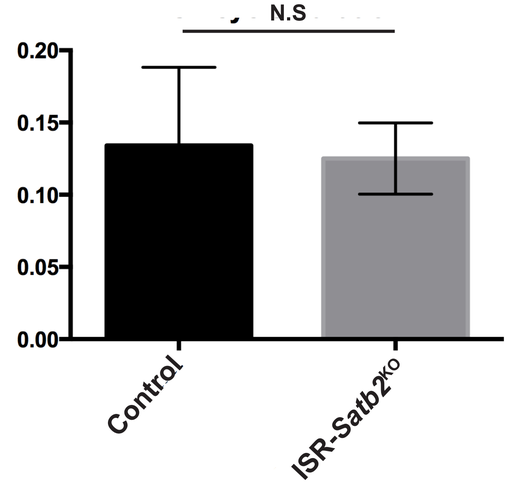

I

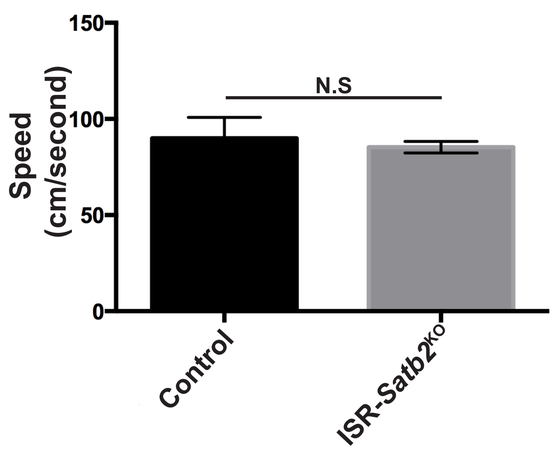

J

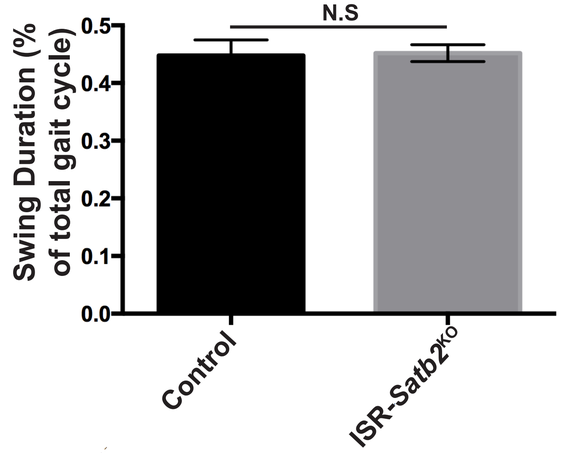

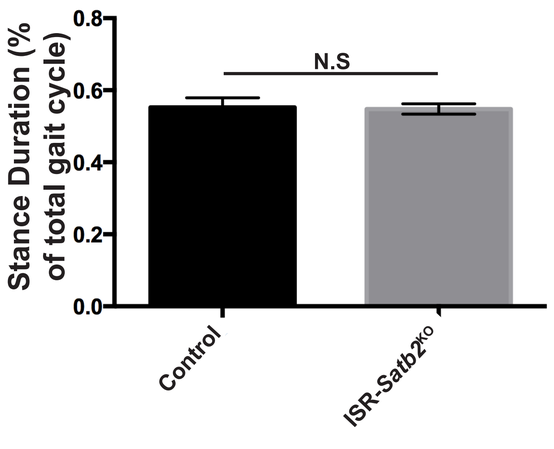

K

Consistency Metrics

	Joint Angle		Step Shape	
	Control	ISR-*Satb2*^{KO}	Control	ISR-*Satb2*^{KO}
mean	93.51797	93.99981	95.92422	96.81424
SEM	1.578984	1.022198	1.596284	0.950558
ci.low	89.98985	91.79339	92.42422	94.66368
ci.high	95.83382	95.65607	98.0562	98.19034

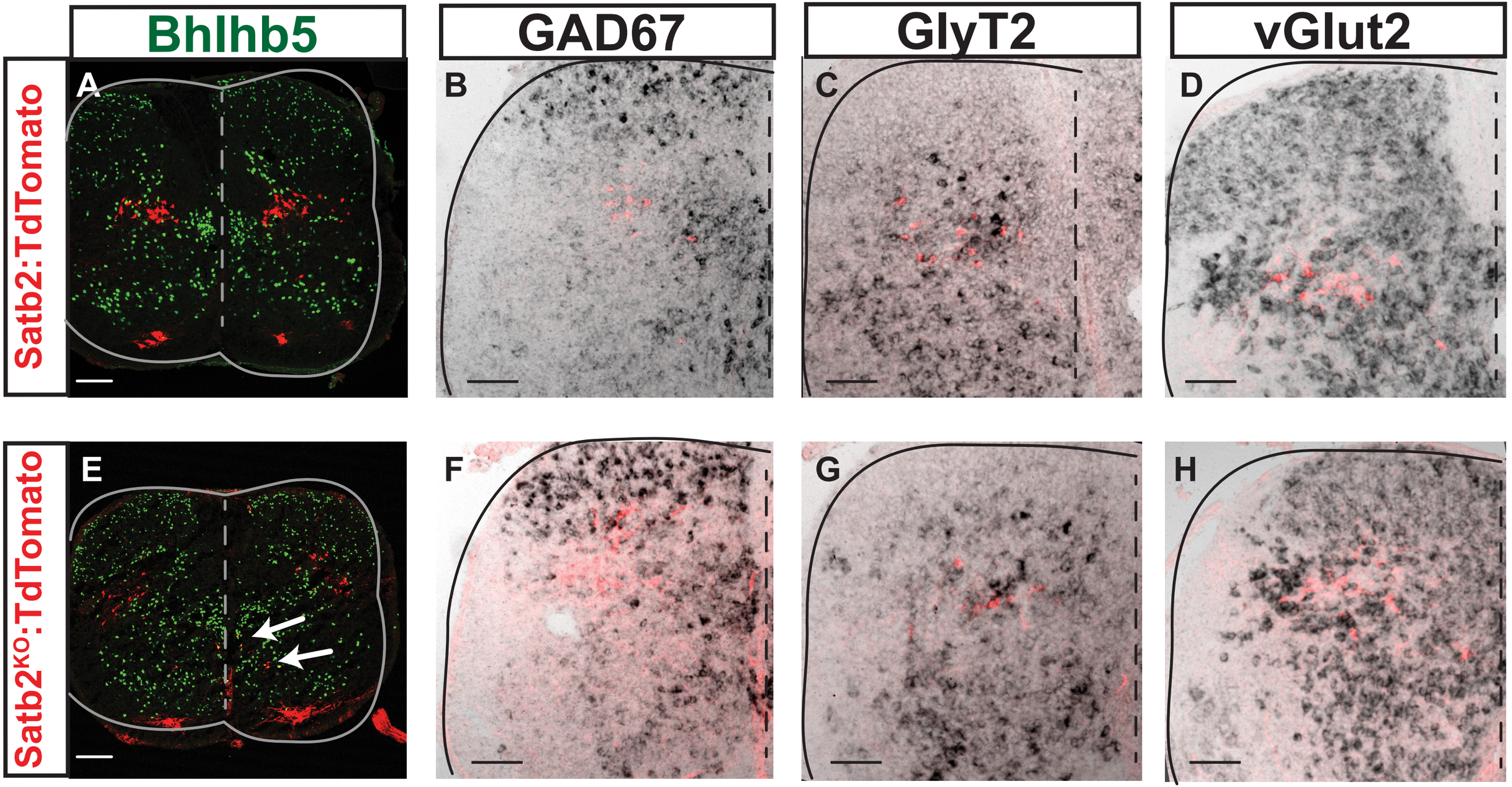
Bhlhb5
GAD67
GlyT2
vGlut2
Satb2:TdTomato
Satb2KO:TdTomato
A
B
C
D
E
F
G
H

Figure S1, Related to Figure 1. Timeline of Satb2 expression in the developing spinal cord

A-F. Immunohistochemistry using a Satb2-directed antibody in the spinal cord at e10.5 (A), e12.5 (B), e13.5 (C), e15.5 (D), P0 (E), and P7 (F). Expression of Satb2 was first identified in spinal interneurons at low levels at e12.5, continuing until P7. Expression in motor neurons was first identified at e10.5 with expression in the medial motor column (MMC). Satb2 was observed throughout the medial and lateral motor columns (LMC) at e12.5, then continued in a subset of MMC motor neurons through embryonic stages. After e15.5, Satb2 expression was rarely observed in motor neurons, but when present, was observed in MMC motor neurons. Representative images show cervical (A, B, C) or lumbar (D, E, F) levels of the spinal cord, though Satb2 expression is detected throughout the rostral-caudal axis. **G, H.** Satb2 antibody labeling (Satb2 Ab) in Satb2:TdTomato spinal cord, e15.5. Satb2:TdTomato labeling demonstrates that our transgenic line is high efficiency and accurately recapitulates Satb2 expression in the spinal cord. Scale bars, 100um.

Figure S2, Related to Figure 1. Satb2 coexpresses Lbx1, Lim1/2, Ptf1a and markers of inhibitory neurotransmitter identity

Co-labeling experiments for Satb2 (red) and lineage markers for dorsal interneuron populations (green). High and low magnification images are shown for each marker for immunohistochemistry. Satb2+ interneurons express Lbx1, Lim1/2, and a subset express Ptf1a. **A, B.** Satb2 antibody and Lbx1:TdTomato, e15.5. **C, D.** Satb2:TdTomato and Lim1/2 antibody, e13.5. **E, F.** Satb2 antibody and Ptf1a:TdTomato, e15.5. **G, H.** Satb2 antibody and Pax2 antibody, e18.5. **I, J.** Satb2 antibody and Bhlhb5 antibody, e18.5. **K, L.** Satb2 antibody and Isl1/2 antibody, e13.5. **M, N,** Satb2 antibody and Lmx1b:TdTomato, e18.5. **O, P.** Satb2 antibody and Brn3a antibody, e13.5. **Q-S**. Satb2 antibody and in situ hybridization for Gad65 (Q), Gad67 (R), and vGlut2 (S) at P13. Arrows indicate Satb2+ interneurons that co-express transcription factor marker or in situ hybridization probes. Scale bars in low magnification immunohistochemistry images, 100um. Scale bars in high magnification immunohistochemistry images, 20um. Scale bars in in situ hybridization images, 100um.

Figure S3, Related to Figure 2, 3. Satb2+ interneuron connectivity

A, B. Proprioceptive connections onto Satb2:TdTomato interneurons were detectable using parvalbumin (PV, green) and vGlut1 (white) immunoreactivity. ISR^{Satb2} neurons are embedded in a dense proprioceptive termination zone. **C, D.** In contrast to the specific, ventral distribution of presynaptic terminals of Satb2+ interneurons (see Figure 3A), Lmx1b- (C) and Ptf1a-expressing (D) dorsal interneurons target dorsal laminae broadly. We also noted glial expression of the fluorescent reporter in D. P29 spinal cords in A, B. **E-G.** Immunohistochemistry of Satb2:Syn-Tom spinal cords for Evx1 (E), Calbindin (F), and Bhlhb5 (G). Presynaptic terminals of Satb2+ interneurons (white) were identified on cell bodies (marked with neurotrace, green) of ventral interneurons (red), as indicated by arrows. **H, I.** Unilateral spinal injection of scAAV-Flex-GFP into Satb2:Cre animals labels ISR^{Satb2} neurons in the neonatal spinal cord (H). Ascending fiber projections were not detected at the level of the brainstem-spinal cord junction (I), an area where fibers from ascending tracts reside. Scale bars in A, C, D, H, I, 100um. Scale bars in B, E-G, 20um.

Figure S4, Related to Figure 4. Strategy for eliminating Satb2 in the developing spinal cord

A-C. Immunohistochemistry (red) for Satb2 antibody in control (A), ISR-*Satb2*^{KO} (B), and Satb2^{KO}:TdTomato (C) spinal cords. **D**. Immunohistochemistry for Lbx1 (green) and Hb9 (blue) antibodies reveals that Satb2 expression does not overlap with Lbx1 in the brainstem. **E.** Immunohistochemistry for Hb9 antibody (green) in Lbx1:TdTomato (red) spinal cords, e14.5. Lbx1-Cre:Rosa-CAG-LSL-TdTomato (Lbx1:TdTomato) labeling revealed a broad expression pattern inclusive of the dorsal spinal cord where ISR^{Satb2} interneurons reside. Importantly, Lbx1:TdTomato expression was not detected in Hb9-expressing motor neurons, the cortex, or limb and facial skeletal structures (data not shown), indicating that use of Lbx1-Cre for behavioral testing is a genetic strategy that excludes other tissue types that normally express Satb2. **F.** In Satb2^{KO}:TdTomato spinal cords, motor neurons in the medial motor column (MMC) maintain the expression of Hb9 (green). Arrowheads indicate expression of

Hb9 in TdTomato+ MMC motor neurons. MMC motor neurons also express additional markers Lhx3, Isl1/2 and have a normal axon trajectory (data not shown). Scale bars in A-D, 100um; Scale bars in E, F, 20um.

Figure S5, Related to Figure 4, 5. Satb2 is not required for normal fictive locomotor activity and crude motor coordination

A, B. Loss of Satb2 does not alter the cycle period or regularity of fictive locomotor activity. A. Cycle period of control (black) and Satb2 null (red) recordings. Cycle period for individuals are shown as dots. Mean +/- SEM is reported for each genotype. B. Cycle period variation of control (black) and Satb2 null (red) recordings. Cycle period variation (cycle period CV) for individuals is shown as dots. Mean +/- SEM is reported for each genotype. **C.** Open field test measured the total distance traveled for Control and *Satb2*-ISR^{KO} animals. Mean +/- S.E.M is reported. Mann-Whitney test did not reach statistical significance (N.S). **D.** Grip Strength test measuring muscle strength in force (grams). Mean +/- S.E.M is reported. Mann Whitney test to compare Control and *Satb2*-ISR^{KO} animals did not reach statistical significance (N.S) at forelimb or hindlimb levels. **E.** Rotarod test for overall motor coordination. Mean +/- S.E.M is reported. Mann Whitney test to compare latency to fall (seconds) for control and *Satb2*-ISR^{KO} animals did not reach statistical significance for any of the 4 trials performed. **F-J.** Kinematic parameters for runway walking. Control and *Satb2*-ISR^{KO} had a comparable stride length (F), step duration (G), CV step duration (H); ratio of swing and stance phases during the gait cycle (I), and body limb speed (J). **K.** The consistency of joint angle and step shape across multiple steps and multiple trials are shown for control and *Satb2*-ISR^{KO} animals. Data in K is presented as a mean percentage +/- S.E.M.

Figure S6, Related to Figure 6. Changes in molecular profile in response to loss of Satb2. A, E. Immunohistochemistry for Bhlhb5 in Satb2:TdTomato (A) or Satb2^{KO}:TdTomato (E). In

Satb2^{KO}:TdTomato spinal cords, TdTomato+ neurons along the dorsal midline upregulate the expression of Bhlhb5 (arrows in E). **B-D, F-H.** In situ hybridization for neurotransmitter markers in Satb2:TdTomato (B-D) or Satb2^{KO}:TdTomato (F-H). See also Figure 6J for quantification for A-H. Scale bars, 100um.

Table S1, Related to Figure 6. Changes in molecular profile in response to loss of Satb2.

Quantification of co-labeling experiments for various lineage and transcription factor markers in Satb2:TdTomato and Satb2^{KO}:TdTomato spinal cord. Satb2:TdTomato and Satb2^{KO}:TdTomato columns report the percentage of TdTomato+ neurons colabeled with marker, and corresponding p-value. Significant changes in gene expression are shown in bold for Ctip2, Bhlhb5, and Pax2 ($p < 0.05$, Mann-Whitney). See also Figure S6.

Video S1, Related to Figure 5. Control animals display normal nociceptive withdrawal reflex (NWR)

In response to Hargreaves thermal pain stimulation, control animals perform a normal NWR behavior.

Video S2, Related to Figure 5. ISR-*Satb2*^{KO} animals maintain flexion posture in response to noxious stimulation.

In response to Hargreaves thermal pain stimulation, ISR-*Satb2*^{KO} animals maintain the limb in a withdrawn position.

	Satb2:TdTomato	$Satb2^{KO}$:TdTomato	p-value
Ctip2	**63.97**	**2.9**	**0.016**
Bhlhb5	**1.9**	**13.8**	**0.016**
Lbx1	77.7	81.04	0.5714
Ptf1a	25.4	34	0.1429
Tlx3	4.105	0.655	0.3333
vGlut2	15.6	18.45	0.99
Gad65	55	40	0.2
Gad67	12.5	13.94	0.9428
GlyT2	44	41.25	0.8
Pax2	**6.3**	**40.2**	**0.016**

Supplemental Experimental Procedures

Mouse Lines

Satb2$^{flx/flx}$ (provided by R. Grosschedl, Max Planck Institute of Immunobiology and Epigenetics), Satb2$^{lacz/lacz}$ (Dobreva et al., 2006), Lbx1-Cre (Sieber et al., 2007), Lmx1b-Cre (provided by R. Johnson, University of Texas), Ptf1a-Cre (Kawaguchi et al., 2002), Parvalbumin-Cre (Jax Strain B6;129P2-Pvalb$^{tm1(cre)Arbr}$/J, Stock#008069), Rosa-LSL-TdTomato (Jax Strain B6;129S6-Gt(ROSA)26Sor$^{tm9(CAG-tdTomato)Hze}$/J, Stock#007905), Rosa-CAG-LSL-Syp-tdTomato-deltaNeo (Jax Strain B6;129S-Gt(ROSA)26Sort$^{tm34.1(CAG-Syp/tdTomato)Hze}$/J, Stock #012570). All mouse work was conducted in accordance with IACUC guidelines.

Generation of Satb2-CreER

A Cre-ER/WPRE/polyA/FRT-neo-FRT cassette was inserted into the ATG of the Satb2 locus. ES cells were electroporated and selected with neomycin. Positive clones were identified using PCR and Southern blot analysis with internal probes for Cre. Embryos were genotyped using primer sequences for Cre, as well as primers spanning the region upstream and downstream from the ATG (primers available upon request). Positive founders were crossed with the FLPe delete mouse line to eliminate the neo cassette. Satb2-CreERΔneo animals were used, referred to in the text as the Satb2:Cre^{ERT2} mouse line. Tamoxifen was dissolved in 100% ethanol at a concentration of 50mg/ml, then diluted 1:100 in sunflower seed oil.

Tamoxifen dosing was performed such that two intraperitoneal injections (3mg/kg) were administered to pregnant females or perinatal pups a minimum of 3 days prior to dissection.

Tissue processing, immunohistochemistry, and in situ hybridization

Spinal cords were dissected in PBS and fixed in 4% PFA in PBS for 1-3 hours, washed in PBS, then washed in 30% sucrose. Spinal cords were then embedded in OCT and cryosectioned at

30um for immunohistochemistry and in situ hybridization, and 50um for quantification of synaptic contacts.

The following primary antibodies were used: rabbit β-gal (Cappel; 1:5000), guinea pig anti-Brn3a (Fedtsova and Turner, 1995), goat anti-Bhlhb5 (Santa Cruz Biotechnology, sc-6045, 1:300), rabbit anti-Calbindin (Swant, CB38, 1:100), rabbit anti c-fos (Santa Cruz Biotechnology sc-52, 1:2000), sheep anti-CGRP (Abcam ab22560, 1:1000), guinea pig anti-Chx10 (Thaler et al., 1999), rat anti-Ctip2 (Abcam ab18465, 1:1000), rabbit anti-Evx1 (Moran-Rivard et al., 2001), goat anti-Foxp2 (Santa Cruz Biotechnology, sc-21069, 1:200), guinea pig anti-Hb9 (Thaler et al., 1999), rabbit anti-Isl1/2 (Tsuchida et al., 1994), rabbit anti-Satb2 (provided by T. Kohwi-Shigematsu and Y. Kohwi, Lawrence Berkeley National Laboratory), rabbit anti-Lbx1 (Gross et al., 2000), rabbit anti-Lim1/2 (Tsuchida et al., 1994), rabbit anti-parvalbumin (Swant PV25, 1:1000), rabbit anti-Pax2 (Invitrogen 716000, 1:1000), rabbit anti-RFP (MBL International, PM005, 1:2000), guinea pig anti-Tlx3 (Muller et al., 2005), guinea pig anti-vGlut1 (Millipore AB5905, 1:5000). For identification of cell bodies when examining synaptic contacts, we used neurotrace staining (Invitrogen N-21483).

In situ probes (GAD65, GAD67, and vGlut2) were provided by Q. Ma (Harvard Medical School). To generate the *in situ* probe for GlyT2, the following PCR primer sequences were used to amplify a 545bp fragment: Forward- GTAGTGTTGGGAACCGATGG; Reverse-AGTCCAAGCGTGAGAAGCAT.

For double labeling experiments in which we examined Pax2 marker expression in Satb2+ interneurons, directly conjugated Pax2 antibody was used (Apex Antibody Labeling Kit, Invitrogen). For double labeling experiments in which we examined lineage marker expression in the absence of Satb2 expression, we compared Satb2:TdTomato and $Satb2^{KO}$:TdTomato spinal cords for all experiments except those involving Ptf1a. In this case, Ptf1a-Cre was used in combination with Rosa-CAG-LSL-TdTomato animals. These mice were crossed into a

Satb2$^{lacZ/lacZ}$ background, and the number of cell colabeled with TdTomato and βGal were quantified. Comparisons between Satb2:TdTomato and Satb2^{KO}:TdTomato were performed at e18.5, unless specified otherwise (see Table S1).

For double labeling experiments in which we identified co-labeling of TdTomato and in situ hybridization probes, immunohistochemistry with anti-RFP primary antibody was performed prior to in situ hybridization. After in situ hybridization, secondary antibody to detect RFP signal was applied, and sections were imaged using bright field and fluorescence microscopy.

Unless otherwise noted, n=3-6 spinal cords for quantification of co-expression in double labeling experiments.

Rabies Virus Preparation and Labeling

Rabies virus preparation was performed as described previously (Levine et al., 2014) with the following modifications. Rabies starter viruses containing either mCherry or GFP were obtained from the Callaway lab (Osakada et al., 2011; Wickersham et al., 2007). For visualization of premotor neurons in Figure 3C, Rabies virus (RabΔG) and AAV:G were mixed 4:1 prior to injections. For visualization of motor neurons processes and soma in Figure 3D, Rabies virus (RabΔG) and PBS were mixed 4:1 prior to injection into multiple hindlimb muscles (tibialis anterior, gastrocnemius, and hamstring). Small volume injections (0.3-1.5ul) were performed in various hindlimb muscles at P0-P1 using a Hamilton syringe. Spinal cords were analyzed at P7.

Unilateral spinal injection of scAAV

Intraspinal injections were performed into the lumbar spinal cord as described previously (Levine et al., 2014). Briefly, a unilateral dorsal laminectomy was performed on neonatal (P1-P2) mouse pups, anesthetized on ice. scAAV-Flex-GFP virus was mixed 1:1 with 40% mannitol. A fine glass needle and a picoSpritzer were used to unilaterally inject 0.25ul of virus at a depth of

~300υm from the dorsal surface of the spinal cord where Satb2+ interneurons reside. Spinal cords were analyzed 6-8 weeks later to allow sufficient time for fluorescent labeling of ascending fiber tracts.

CTB labeling of proprioceptive afferents

Intramuscular injections of 1% Cholera Toxin Subunit-B, Alexa Fluor 488 conjugate (CTB; Invitrogen; diluted in sterile saline) were performed into the tibialis anterior muscle of adult animals. 5 injections of 1.5-2ul CTB were performed across the injected muscle. In experiments where CTB labeling was used in combination with c-fos immunohistochemistry (Figure 2E), animals were injected with capsaicin 5 days after the initial CTB injection.

C-fos induction

Capsaicin (Sigma; 0.1% in Ethanol) was injected subcutaneously into the plantar surface of the foot in adult animals. Animals were perfused after 90 minutes and spinal cords were taken for immunohistochemistry. Sections were selected for quantification based on the peak labeling of c-fos in lumbar levels of the spinal cord.

Behavioral Testing

All behavioral testing was conducted according to procedures approved by the Salk Institute IACUC. For all behavioral testing animals were habituated in the testing room for 1 hour prior to the start of the test. Adult animals were used (16-24 weeks of age; male and female) for all behavioral analysis.

Open Field Test

The open field test was performed by observing animals in clear chambers (40.6 x 40.6 x 38.1cm) containing infrared beams to measure horizontal movement. The overall locomotor activity was

measured over a 60 minute time period. The distance traveled was analyzed and the mean+/-SEM is reported. n=14 for control, n=12 for ISR-*Satb2*^{KO}.

Rotarod

Animals were trained on a rotarod for 1 minute at 3rpm, then performed 4 trials in which the rotarod was accelerating from 0-50rpm over 5 minutes. Trials were separated by 10 minutes. The latency to fall was recorded for each individual for 4 trials, and the mean+/-SEM for each trial is reported. n=17 for ISR-*Satb2*^{KO}, n=20 for control (Cre-) littermates.

Hindlimb Grip Strength

A digital grip strength meter (San Diego Instruments) was used to measure force (grams) of mouse forelimb and hindlimb grip response. For hindlimb measurements, animals were positioned to avoid contact of the forelimbs with the meter and to maximize grip reflex of the hindlimb. 5 trials were performed for each animal and the 3 maximum trials were averaged. n=11 for ISR-*Satb2*^{KO}, n=11 for control (Cre-) littermates. Mean+/-SEM for each genotype is reported,

Kinematic analysis of gait

Reflective joint markers were custom designed, and placed on hindlimb joints according to anatomical landmarks (iliac crest, hip, knee, shin, heel and the base of the 5th metatarsal). Animals were trained to walk on a 3cm wide elevated runway apparatus at a steady pace. Individual trials were video-recorded using 4 high speed cameras (mv Blue Cougar XD; 425f/s). Minimum criteria for joint tracking analysis included 2 trials per individual in which at least 5 consecutive steps were recorded. Step consistency metrics were calculated to ensure that representative steps were included for each individual (see below). Swing onset was designated as the time at which the foot left the runway. Stance onset was designated as the time at which the foot contacted the runway.

Joint markers were tracked in 3-dimensions using the Simi Motion Analysis System. Joint angle measurements, limb reconstructions, and limb endpoint trajectories were calculated using a custom R script. Individual joint angles across the gait cycle represent the average of the 2 trial level averages per individual. Genotyped-averaged joint angles are also presented: n=7 control, n=6 ISR-*Satb2*^{KO}.

Statistical analysis of joint angle differences were performed at early swing (1st half of swing), late swing (2nd half of swing), early stance (1st half of stance), and late stance (2nd half of stance). The data were averaged per trial, per animal and finally per group with propagated error from each stage of aggregation. At each aggregation the propagated error is the observed variance divided by the number of observations. If there was a previous level of estimation error then the average of those errors is added to the current level of error. Trial level averages were taken as the coefficients of an ordinary least squares regression of the per-step data against trial level factors. Sample level averages were calculated by weighted least squares regression of the trial level means against sample level factors. The weights were taken as the inverse observed standard error of the mean of each coefficient from the trial level regression. The squared observed standard error of the mean for trial coefficients was added to the residuals as a way to incorporate the errors of the dependent variables in the regression. The final group level means and subsequent statistical test between conditions was generated by weighted least squares regression of the sample level coefficients. Weights were again taken as the inverse standard error of the mean of the sample coefficients and the square error of the mean of sample coefficients was incorporated into the final residuals. The change in mean value between conditions as well as t-statistics and p-values were extracted from the final models.

Stride length was calculated based on the horizontal displacement of the limb between two consecutive gait cycles (swing onset to swing onset). Step duration was calculated based on the amount of time between two consecutive gait cycles (swing onset to swing onset). CV-Step duration is the standard deviation of step duration divided by the mean step duration within a

trial. Body limb speed represents the stride length divided by the step duration. Swing/Stance ratios were determined based on the timing of swing onset/offset for each of the gait cycles analyzed. Consistency metrics were calculated per trial. For joint angle consistency the hip, knee and ankle angle data per step, grouped by trial, were transformed with principal component analysis (PCA). The relative variance captured by the first component was taken as the consistency value for that trial. Final joint angle consistency values represent the average of hip, knee and ankle consistencies for all individuals per condition. Step shape consistency was quantified using the same method as for joint angle using the tracked position of the foot relative to the hip, per step.

Hargreaves Thermal Pain Test

Animals were habituated in a plastic container on a glass surface. Thermal pain was induced using a radiant heat beam (IITC). Intensity of the heat beam was adjusted so that the withdrawal response occurred within a range of ~3-8 seconds. A maximum of 20 seconds was applied to prevent tissue damage. 2 trials were performed on each hindlimb, and an average of left and right hindlimb (4 trials total) was used for each individual. Latency measurements, n=9 for ISR-*Satb2*^{KO}, n=7 for control (Cre-) littermates. Examination of the withdrawal response revealed the normal withdrawal behavior in which animals replaced the limb following painful stimulation. Identification of the maintained flexion posture was assigned as a binary response (maintained flexion or normal response).

Von Frey

Animals were habituated in a plastic container on a wire mesh surface. The threshold for mechanical pain was measured using Von Frey filaments (0.008-2.0g). 5 trials were performed on each hindlimb. Threshold was assigned based on whether the animal responded greater than 50% of the time (3/5 trials or greater). The average of left and right hindlimb was used for each

individual. n=7 for ISR-*Satb2*^{KO}, n=9 for control (Cre-) littermates. Examination of the withdrawal response revealed the normal withdrawal behavior in which animals replaced the limb following painful stimulation. Identification of the maintained flexion posture was assigned as a binary response (maintained flexion or normal response).

Light Touch

Animals were habituated in a plastic container on a wire mesh surface. The footpads of test animals were stimulated with longitudinal brush strokes. 5 trials were performed on each hindlimb, and paw withdrawal frequency is presented as a percentage of trials that elicited a withdrawal response. Paw withdrawal frequency represents the 10 trials performed for each animal (5 trials per hindlimb). n=9 for control (Cre-) littermates, n=9 for ISR-*Satb2*^{KO}. Identification of the maintained flexion posture was assigned as a binary response (maintained flexion or normal response).

Fictive Locomotion Experiments

Fictive locomotion experiments were performed as described previously (Myers et al., 2005) with the following modifications. Lumbar spinal cords of e18.5 embryos were dissected in cold dissecting ACSF (128 mM NaCl; 4 mM KCl; 21 mM $NaHCO_3$; 0.5 mM NaH_2PO_4; 3 mM $MgSO_4$; 30 mM d-glucose; and 1 mM $CaCl_2$) oxygenated with 90% O_2/ 5% CO_2. Dissected spinal cords were transferred to room tempereature oxygenated recording solution (128 mM NaCl; 4 mM KCl; 21 mM $NaHCO_3$; 0.5 mM NaH_2PO_4; 1 mM $MgSO_4$; 30 mM d-glucose; and 2 mM $CaCl_2$). Locomotor activity was induced by bath application of 20uM serotonin (5-HT), 10um N-methyl-D, L-aspartate (NMA). Motoneuron activity was recorded from the ventral roots with suction electrodes, amplified 1000x and filtered from 100Hz-3kHz The activity of left and right L2 ventral roots were recorded for contralateral phase comparisons, and ipsilateral L2 and

L5 ventral roots for ipsilateral flexor extensor phase comparisons. Analysis of fictive locomotor activity phase and cycle period was conducted offline with custom written scripts in R. Satb2 null ($Satb2^{lacZ/lacZ}$) and control littermates were used. n=7 for Satb2 null, n=4 for control.

Pixel Intensity Quantification

Spinal cords from Satb2:Syn-Tom and $Satb2^{KO}$:Syn-Tom animals were sectioned and immunohistochemistry for RFP was performed simultaneously. Pixel intensities were mapped along the dorso-ventral axis using the plot profile function of ImageJ software to correspond pixel intensity to distance along the dorsoventral axis. Hemicords were used for region of interest (ROI) for plot profiles. The dorsoventral distance of the spinal cord was normalized to the average of the population in order to correct for variability of section size. n=5 for $Satb2^{KO}$:TdTomato, n=6 for Satb2:TdTomato

Identification of synaptic contacts and quantification of synaptic input

Individual synaptic contacts were identified based on colocalization between TdTomato+ presynaptic terminals and neurotrace+ cell bodies by examining images of high magnification single focal planes.

To visualize proprioceptive contacts, spinal cords from Parvalbumin:Syn-Tom animals were sectioned and immunohistochemistry for Satb2 and neurotrace was performed. Thick (50um) sections were imaged at high resolution. Cells for quantification were selected based on whether the entire cell body was captured in the image stack. Individual synaptic contacts were identified based on colocalization between presynaptic terminals and neurotrace+ cell bodies of Satb2+ interneurons by examining serial image slices. The number of synaptic contacts were then binned and correlated to mediolateral position.

In some cases, parvalbumin and vGlut1 colocalization was used to identify proprioceptive contacts on cell soma and processes of Satb2:TdTomato interneurons. In experiments that

identified proprioceptive inputs onto Satb2:TdTomato neurons that are activated following capsaicin injection (Figure 2E), CTB/vGlut1 colocalization was identified with ImageJ.

Supplemental References:

Dobreva, G., Chahrour, M., Dautzenberg, M., Chirivella, L., Kanzler, B., Farinas, I., Karsenty, G., and Grosschedl, R. (2006). SATB2 is a multifunctional determinant of craniofacial patterning and osteoblast differentiation. Cell *125*, 971-986.

Fedtsova, N.G., and Turner, E.E. (1995). Brn-3.0 expression identifies early post-mitotic CNS neurons and sensory neural precursors. Mechanisms of development *53*, 291-304.

Gross, M.K., Moran-Rivard, L., Velasquez, T., Nakatsu, M.N., Jagla, K., and Goulding, M. (2000). Lbx1 is required for muscle precursor migration along a lateral pathway into the limb. Development *127*, 413-424.

Guo, T., Mandai, K., Condie, B.G., Wickramasinghe, S.R., Capecchi, M.R., and Ginty, D.D. (2011). An evolving NGF-Hoxd1 signaling pathway mediates development of divergent neural circuits in vertebrates. Nature neuroscience *14*, 31-36.

Kawaguchi, Y., Cooper, B., Gannon, M., Ray, M., MacDonald, R.J., and Wright, C.V. (2002). The role of the transcriptional regulator Ptf1a in converting intestinal to pancreatic progenitors. Nature genetics *32*, 128-134.

Levine, A.J., Hinckley, C.A., Hilde, K.L., Driscoll, S.P., Poon, T.H., Montgomery, J.M., and Pfaff, S.L. (2014). Identification of a cellular node for motor control pathways. Nature neuroscience *17*, 586-593.

Moran-Rivard, L., Kagawa, T., Saueressig, H., Gross, M.K., Burrill, J., and Goulding, M. (2001). Evx1 is a postmitotic determinant of v0 interneuron identity in the spinal cord. Neuron *29*, 385-399.

Muller, T., Anlag, K., Wildner, H., Britsch, S., Treier, M., and Birchmeier, C. (2005). The bHLH factor Olig3 coordinates the specification of dorsal neurons in the spinal cord. Genes & development *19*, 733-743.

Myers, C.P., Lewcock, J.W., Hanson, M.G., Gosgnach, S., Aimone, J.B., Gage, F.H., Lee, K.F., Landmesser, L.T., and Pfaff, S.L. (2005). Cholinergic input is required during embryonic development to mediate proper assembly of spinal locomotor circuits. Neuron *46*, 37-49.

Osakada, F., Mori, T., Cetin, A.H., Marshel, J.H., Virgen, B., and Callaway, E.M. (2011). New rabies virus variants for monitoring and manipulating activity and gene expression in defined neural circuits. Neuron *71*, 617-631.

Sieber, M.A., Storm, R., Martinez-de-la-Torre, M., Muller, T., Wende, H., Reuter, K., Vasyutina, E., and Birchmeier, C. (2007). Lbx1 acts as a selector gene in the fate determination of somatosensory and viscerosensory relay neurons in the hindbrain. The Journal of neuroscience : the official journal of the Society for Neuroscience *27*, 4902-4909.

Thaler, J., Harrison, K., Sharma, K., Lettieri, K., Kehrl, J., and Pfaff, S.L. (1999). Active suppression of interneuron programs within developing motor neurons revealed by analysis of homeodomain factor HB9. Neuron *23*, 675-687.

Tsuchida, T., Ensini, M., Morton, S.B., Baldassare, M., Edlund, T., Jessell, T.M., and Pfaff, S.L. (1994). Topographic organization of embryonic motor neurons defined by expression of LIM homeobox genes. Cell *79*, 957-970.

Wickersham, I.R., Finke, S., Conzelmann, K.K., and Callaway, E.M. (2007). Retrograde neuronal tracing with a deletion-mutant rabies virus. Nature methods *4*, 47-49.